A Technique to Determine Lift and Drag Polars in Flight

A. Knaus*
Messerschmitt-Bölkow-Blohm GmbH, Munich, Federal Republic of Germany

Performance trials of the European combat aircraft Tornado have concentrated on the systematic measurement of lift and drag polars. Such polars have been successfully measured by means of well-adapted test instrumentation, a data reduction system, and a high calibration standard of the aircraft and engines. The use of a certain combination of steady-state and dynamic test maneuvers has resulted in a drastic reduction in the amount of flight time required to obtain sufficient data for the determination of the zero lift drag, induced drag characteristics, and drag increments due to aircraft configuration changes. Flight test results are presented which demonstrate the advantage of the utilized test technique and the high data quality achieved.

Nomenclature

A_7 = nozzle exit area calculated
A_j = nozzle exit area measured
AX_D = acceleration along flight path
AZ_L = acceleration normal to flight path
AX_{NC}, AY_{NC}, AZ_{NC} = acceleration corrected
C_D, C_L = coefficient of drag and lift, respectively
C_G = gross thrust coefficient
C_{DN} = nozzle discharge coefficient
c.g. = center of gravity
D = drag
D_R = ram drag
F_{ex} = excess thrust
F_G = gross thrust
F_{Gid} = gross thrust ideal (calculated)
F_N = net thrust
g = gravitational constant
K_1, K_2 = angle-of-attack calibration coefficients
L = lift
MF_M = main fuel mass flow
MF_R = reheat fuel mass flow
M_T = Mach = true Mach number
M_1 = air mass flow at engine entry
M_6 = gas mass flow at nozzle entry
M_7 = gas mass flow at nozzle exit
M_{BL} = bleed mass flow
N_H = high-pressure spool speed
n_z = load factor
P_{So} = ambient pressure
P_{mix} = mixed total pressure (from PT_4+PT_{4LB})
P_j = measured total pressure at nozzle exit
PT_1 = total pressure at engine entry
PT_4 = total pressure at low-pressure turbine exit
PT_{4LB} = total pressure at bypass exit
POT = power off take
p = roll rate
q = pitch rate
r_x = angle-of-attack sensor x axis distance to c.g.
r_y = angle of attack sensor y axis distance to c.g.
S.L. = sea level
t = time
TT_1 = freestream total temperature
TT_5 = mixed jet pipe entry temperature
V_T = true airspeed
V_7 = nozzle exhaust speed
W = weight
α_E = corrected true angle of attack
α_i = indicated angle of attack
β = angle of sideslip
γ = angle of flight path
ΔA_7 = nozzle area correction
ΔP = $P_{mix}-P_j$
Λ = angle of wing sweep
σ = angle of engine installation

Presented as Paper 81-2420 at the AIAA/SETP/SFTE/SAE/ITEA/IEEE 1st Flight Testing Conference, Las Vegas, Nev., Nov. 11-13, 1981; submitted Nov. 16, 1981; revision received Oct. 22, 1982.

*Head of Flight Test Analysis, Flight Test Department.

Introduction

THE determination of the performance capability of a newly developed combat aircraft during flight testing is of great importance. The purpose of aircraft performance trials is to obtain characteristic performance data for the entire mission spectrum. These data are needed in order to compare flight test derived results with predicted data, to determine the performance capability of the aircraft, and to provide evidence of this capability to the customer.

As a rule, when a new aircraft project is being developed, the first phase of testing is carried out on prototypes with an airframe and a powerplant system which, in most cases, are not completely identical to those in the final production aircraft. For this reason, the accurate measurement of engine thrust and the establishment of the lift and drag polars should be given priority from the very beginning.

Thus, in the course of flight testing, the aerodynamic qualities of the airframe and the effectiveness of the power system can be determined and analyzed systematically. These considerations were of particular importance in the case of the European combat aircraft Tornado.

On the one hand, flight testing on the newly developed RB 199 three-spool engine has been started simultaneously with aircraft testing. The result was that most of the aircraft performance trials had to be carried out with engines whose performance characteristics were not identical to those of production engines. On the other hand, the aerodynamic configuration of the first prototypes was not identical to that of the final production aircraft.

Wind-tunnel tests had already revealed that various modifications had to be flight tested so as to optimize the airframe. Beyond that, a large number of different aircraft configurations had to be tested within an extensive Mach, altitude, and normal acceleration envelope.

Therefore the objective of Tornado performance trials was to determine the performance characteristics by means of an economic test method which ensures high-quality data, and to evaluate and analyze the test results within a short time period.

This paper gives a general overview of the methods and techniques which were used to measure the Tornado lift and drag polars, and it also presents typical test results. The thrust in-flight measurement method used in this context is briefly discussed, but a more detailed description is given in Ref. 1.

Test Aircraft

The design of the two-seat Multi Role Combat Aircraft Tornado is characterized by its compact fuselage and shoulder mounted variable geometry wing, and its low taileron and relatively tall vertical fin. A three-view drawing of the airplane is shown in Fig. 1. The sweep range of the wing is from 25 to 67 deg and can be manually controlled in flight. Lift augmentation for takeoff, landing, and maneuvering is provided by full-span leading-edge slats, double-slotted trailing-edge flaps, and Krüger flaps on the highly swept fixed-wing gloves. Two speed brakes with an automatic blowback system are located on the upper side of the rear fuselage.

A wide range of external stores can be carried on a total of seven pylons: three pylons under the fuselage and, under the movable wings, two swiveling pylons each.

The air intake system consists of two horizontal two-dimensional variable geometry inlets with three ramps. Ploughshare shaped boundary-layer diverters separate the intake from the fuselage side. An inlet throat bleed hood is located on the top of each intake for ramp boundary-layer control and inlet air bypass. Furthermore, two blow-in auxiliary doors are on the side of each intake in order to achieve high-pressure recovery under takeoff conditions.

The aircraft is powered by two RB199-34R engines, developed by the trinational consortium Turbo-Union. The RB199 is a three-spool bypass engine, designed for high thrust under takeoff and combat conditions and for low fuel consumption in high subsonic flight at low altitudes. Figure 2 shows a schematic cutaway view of the engine.

The three-stage fan is driven by a two-stage low-pressure (LP) turbine. A three-stage intermediate-pressure (IP) compressor is driven via a separate shaft by a single-stage IP turbine, and the six-stage high-pressure (HP) compressor is driven by a single-stage HP turbine.

The reheat system combines a conventional turbojet burner with gutter flame stabilizers for the hot turbine efflux and a separately fueled colander burner for the bypass flow. The variable, convergent exhaust nozzle consists of 14 pairs of interlocking primary and secondary petals. The nozzle area varies from a minimum of 0.208 to 0.4 m^2 at maximum reheat.

Bucket-type thrust reversers, developed to fulfill the requirements for extremely short landing distances, are mounted at the rear of the engine.

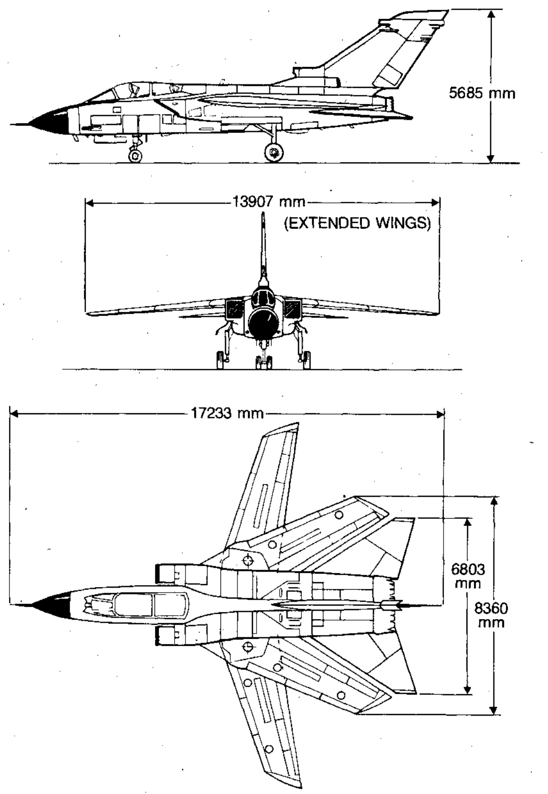

Fig. 1 Three-view drawing of Tornado.

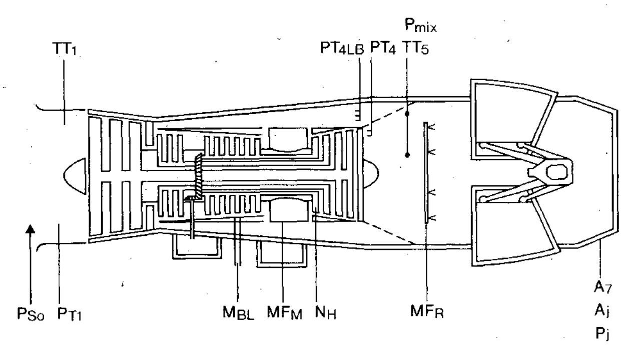

Fig. 2 Thrust in-flight engine instrumentation.

Test Equipment

All test aircrafts involved in Tornado performance testing were equipped with flight test instrumentation of high quality which also contained parameters for stability/control and propulsion systems flight testing. The instrumentation system has the capability to record all data on magnetic tape and to telemeter it to the ground station, equipped with a data reduction system for real-time analysis.

The onboard data acquisition system consisted of a Pulse Code Modulation System (PCM) on a Frequency Modulation-Multiplex System (FM/FM) to record and transmit digital and/or analog signals. It also included units for signal conditions, filtering, and timecoding.

The entire measuring chain of each individual performance parameter was calibrated and continuously monitored during the performance test phase in order to achieve the required test data accuracy. Particular emphasis was placed on the accurate measurement of 1) total and static pressures, angle of attack, and sideslip by means of a specially developed noseboom with wind vanes; 2) longitudinal, lateral, and normal acceleration using thermally controlled sensitive accelerometers which were accurately aligned and installed close to the center of gravity of the aircraft; and 3) specific engine parameters such as pressures, temperatures, fuel flow, etc., as shown in Fig. 2, which are required for the determination of engine thrust in-flight.

Engine calibration data (for example, discharge coefficient, thrust coefficient, pressure loss in the afterburner tailpipe, etc.) used in conjunction with in-flight measured engine parameters for the calculation of engine mass flow and net thrust, were obtained from special component test beds or from altitude test facilities (ATF). Engines used for performance trials were generally calibrated in the ATF at the National Gas Turbine Establishment (NGTE) in Pyestock, U.K.

Performance Test Program

The objectives of the test program were to ensure that the performance requirements of the customer would be fulfilled by the production aircraft, to demonstrate this, and to establish all performance data required for the Flight Manual. To meet these objectives, comprehensive performance trials over more than six years on two prototypes and two preseries aircraft were conducted as shown in Fig. 3.

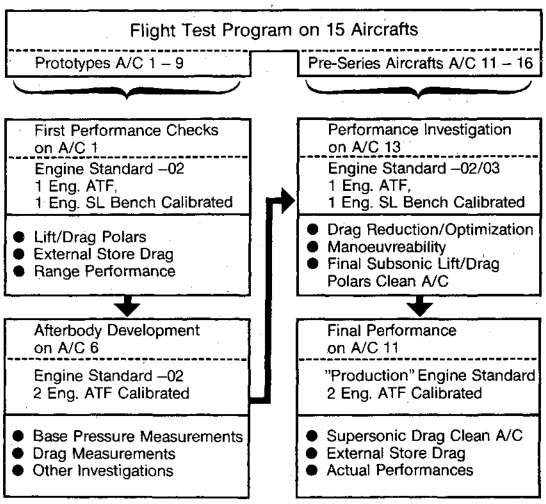

Fig. 3 Tornado performance test program.

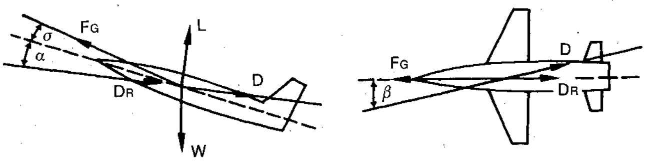

Fig. 4 Forces on airplane.

As one can see, the performance investigations concentrated mainly on establishing the lift and the drag of the aircraft. Because of this it was possible to continuously verify in-flight the effects due to aerodynamic modifications and to provide a dependable forecast as to the performance capability of production aircraft at the earliest possible date.

Background

During flight test, the lift and drag of the total aerodynamic force cannot be measured directly; however, they can be calculated from measurable quantities. This is illustrated below, showing the forces which act on the aircraft. The lift and drag can be expressed as follows (also, see Fig. 4):

$$L = -F_G \sin(\alpha_T + \sigma) + (W/g)\, AZ_L$$

$$C_L = L/Sq$$

$$D = F_G \cos(\alpha_T + \sigma)\cos\beta_T + F_G \sin\beta_T$$

$$-D_R \cos\beta_T + (W/g)\, AX_D$$

$$C_D = D/Sq$$

The engine installation angle σ and the wing reference area S are fixed, known geometric quantities. The dynamic pressure q can readily be obtained. It can be seen that the lift and drag are dependent on the gross thrust F_G, the intake ram drag D_R, the aircraft weight W, the longitudinal acceleration AX_D, and the normal acceleration AZ_L, as well as the actual angle of attack α_T and the angle of sideslip β_T. These remaining quantities are discussed in the following sections.

In-Flight Thrust Measurement

The so-called "thrust derived P_j/nozzle calibration" method as the main method for gross thrust and mass flow determination was developed in cooperation with the engine manufacturer.[1] This method avoids problems due to distorted flow profiles at the engine face by utilizing engine parameters at the nozzle exit. A further important point is that the same instrumentation is used as well in-flight as during engine calibration.

The engine gross thrust F_G and ram drag D_R are defined as follows:

$$F_G = F_{\text{Gid}} \times C_G \qquad D_R = M_1 \times V_T$$

The ideal gross thrust F_{Gid} is calculated from thermodynamic parameters in the nozzle exit plane which are obtained from in-flight measured parameters and from engine ATF calibration. For example, the nozzle exit pressure PT_7 is calculated from measured PT_4 and PT_{4LB} pressures (area weighted, see Fig. 2) and from pressure drop Δp obtained during engine calibration. Thus

$$F_{\text{Gid}} = f\,(M_7, V_7, A_7, P_{\text{mix}}, \Delta P, P_{So})$$

The determination of the mass flow M_6 at the nozzle entry is based on an overall engine heat balance, which includes measured and calculated engine parameters:

$$M_6 = f(\text{fuel energy}, MF_M, MF_R, \text{POT}, TT_1, TT_5, M_{BL})$$

and thus the mass flow at the engine face

$$M_1 = M_6 + M_{BL} - (MF_M + MF_R)$$

The main feature of this method is nozzle matching; i.e., the calculation loop for thrust and mass flow will continue as long as the measured nozzle area A_j minus ΔA_7 is equal to the calculated (aerodynamic) nozzle area A_7:

$$M_{7(\text{new})} = M_{7(\text{old})}\,(A_j/A_7)\; C_{DN}\,(1 - \Delta A_7/A_j)$$

ΔA_7 is obtained from a calibration curve established from ATF data.

Finally the in-flight engine thrust resulting from this method is adjusted to the defined Tornado thrust/drag bookkeeping system. This means that drag components such as subcritical spill drag and nozzle interference drag, which are functions of engine rating and flight condition, are accounted for within the thrust term. These drag items have been obtained from wind-tunnel tests with special intake and propulsion nozzle/afterbody models. Hereby the polars have been made completely independent of induced drag effects due to engine rating.

Aircraft Acceleration Measurement

For use in the basic equations, the total inertia force must be split into components along and normal to the flight path (AX_D and AZ_L). The load factor and the excess thrust can be derived from

$$n_z = AZ_L/g \qquad F_{\text{ex}} = AX_D\,(W/g)$$

Accelerations can be determined by two different methods: 1) the "classic" *total energy method* for stabilized flight conditions, and 2) the *accelerometer method* mainly for dynamic flight conditions.

The *total energy method* makes use of pitot/static system indications only and gives the accelerations directly in the required lift/drag axis.

AX_D is determined via the residual rate of change of altitude and speed ($\mathrm{d}H$, $\mathrm{d}V_T$) over the stabilized part ($\mathrm{d}t$) of the maneuver:

$$AX_D = \frac{\mathrm{d}V_T}{\mathrm{d}t} + \frac{\mathrm{d}H}{\mathrm{d}t} \times \frac{g}{V_T}$$

The normal acceleration AZ_L is calculated via the flight-path angle γ, a rectilinear trajectory supposed:

$$AZ_L = g\cos\gamma$$

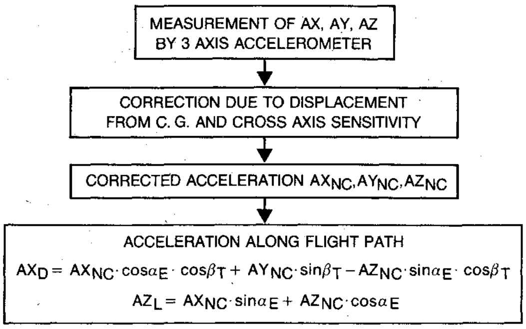

Fig. 5 Accelerometer method.

where γ is derived from

$$\sin\gamma = \frac{dH}{dt} \bigg/ V_T$$

The "classic" maneuver for the application of this method is the steady level; however—to a certain extent—accelerations/decelerations and climbs/descents at constant rates can be evaluated as well. Excess thrust is determined with a high degree of accuracy.

The accelerometer method uses the readings of an accelerometer package for the three aircraft axes. After a correction for cross-axis sensitivity, the measured accelerations have to be transfered from the location of the sensors to the center of gravity and then from the body—into the aerodynamic (lift/drag) system of axes.

The transformations were done by the use of standard equations which might be modified if the sensors measure in any other than the body axes (for example, in the geodetic system as with an inertial navigation platform). The resultant equations, as used in the data reduction, are given in Fig. 5 in terms of AX_D and AZ_L.

Angle-of-Attack and Sideslip Measurements

The angle of attack was measured by a noseboom mounted wind vane or by a fuselage mounted differential pressure probe.

A final accuracy of $\alpha_T = \pm 0.1$ deg is mandatory and this requires a careful calibration which considers the following factors:

1) correction for local flow and upwash effects from in-flight calibration ($\alpha_p = K_1 + K_2 \times \alpha_i$),

2) pitch (roll) rate correction

$$\Delta\alpha_q = \arcsin(q\,V_x / V_T) \qquad \Delta\alpha_r = \arcsin(p\,r_y / V_T)$$

3) fuselage and noseboom bending due to air and inertia loads $\Delta\alpha_B$ (from static structural tests and in-flight calibration),

4) correction due to inclined installation of the sensor ($\Delta\alpha_M$).

This finally leads to the true angle of attack for a given Mach number:

$$\alpha_T = k_1 + k_2 \times \alpha_i + \Delta\alpha_q + \Delta\alpha_r + \Delta\alpha_B + \Delta\alpha_M$$

In a similar way the sideslip can be determined; however, the main interest during lift/drag measurements is a correct indication of a zero sideslip, as the test maneuver should be carried out at zero sideslip.

Table 1 Flight maneuvers for the polar evaluation

Maneuver	Procedure	Region of applicability test conditions	Test results
Accel-decel-accel, dynamic maneuver in the vertical plane by a lift variation due to a speed variation	Start maneuver in level flight; decelerate/accelerate A/C by stick inputs with constant power	Lower-speed range, power approach configuration	Several polar points per test in the neighborhood of the trim point
Slow-down, deceleration to high angle of attack	Start maneuver in level flight; decelerate by pulling up slowly to maximum angle of attack; keep power lever constant	Low-speed range, especially in maneuver, start, and landing configuration	Several polar points up to maximum angle of attack
Level acceleration or deceleration	Acceleration (deceleration) of initial to target speed at constant altitude	At any speed, altitude, and configuration	Especially for drag-rise evaluation and influence of nozzle positions
Steady level	A/C trimmed for $1g$ level flight at test speed and altitude; hold speed and altitude constant and stabilize for 2 min	At any speed and altitude, however uneconomical, particularly in supersonic	1 polar point per test
Roller-coaster or pushover/pullup dynamic maneuver in the vertical plane with load factor variation between 0 and $2g$.	Push-over slowly from 1 to $0g$; then pull up slowly to $2g$; thrust is constant and Mach excursion should be kept as low as possible	(Clean wing) flaps retracted; Mach = 0.4-0.95	Several polar points around the trim point; lift range 0-$2g$, especially for the determination of C_{D_0}
Wind-up turn, dynamic performance maneuver with load factor variation between $1g$ and maximum g	Start initial banking 2000 ft above test altitude; increase load factor by pulling up slowly; maintain speed by reducing altitude, but constant power lever	At any altitude and speed, Mach > 0.4; favorite maneuver in supersonic	Several polar points from $1g$ to maximum g per test

Aircraft Mass and Center of Gravity Determination

The actual gross weight, W, and c.g. are calculated from the empty weight and the fuel contents in the individual tank groups. Aircraft empty mass and the corresponding c.g. were determined by weighing. The actual contents of the fuel tank groups was measured in-flight by fuel gages which were calibrated for various attitude angles on a special fuel rig.

Test Technique

The need for a cost-effective test procedure and an accurate method for determining lift and drag polars over a large angle-of-attack range at a constant Mach number requires the use of various dynamic maneuvers in combination with steady levels. The flight maneuvers which were used in testing are tabulated and described in Table 1.

Depending on the aircraft configuration and the Mach range to be covered, the following maneuver sequence was performed.

Cruise, Maneuver, and High-Speed Polars

After a steady level flight of from 2 to 2.5 min duration, the range of angle of attack (corresponding to a load factor of from 0 to $2g$) about the trim point is covered by means of a roller coaster maneuver. After this maneuver, the aircraft is stabilized briefly and then the range of greater incidence angle (corresponding to a load factor of from $1g$ to maximum g) is tested by means of a wind-up turn maneuver. Using this combination, it is possible to obtain the flight data for the entire incidence range within 3 to 4 min.

Another advantage of this method is the chance of comparing continuously the results obtained from different types of flight maneuvers. Thus possible measuring errors (shifts, offsets) can be detected more easily and more quickly, and even small residual errors in the measurements or alignment of the accelerometers can be verified.

A test flight can cover a large number of such maneuver sequences when higher or lower test Mach numbers are joined by accelerations or decelerations, as shown in Fig. 6. This test technique produces further test data and allows, in addition, the verification of the drag rise and the zero lift drag.

Low-Speed Polars (Takeoff-Landing Configuration)

In the range below $Ma = 0.4$ acceleration-deceleration-acceleration and slow-down maneuvers were used instead of roller-coaster or wind-up maneuvers because in this range Mach effects on the polars are negligible and the aircraft can be piloted better. Again, these maneuvers are carried out after a steady level flight of from 2 to 2.5 min duration.

The accel-decel-accel maneuver is used for testing the range of angle of attack about the trim point and the slow-down maneuver, for the range up to the maximum permissible angle of attack. Consequently, the entire polar can be flown within approximately 5 min.

Using this test method it was possible, for example, in the course of Tornado testing, to establish a complete set of subsonic polars within a 1-h test flight. Without using dynamic test maneuvers, the flight time required to obtain test data even for a limited range of angle of attack would be at least from 4 to 5 times greater.

Furthermore, it is evident that conventional steady level maneuvers do not allow collection of enough data points for the determination of induced drag and zero lift drag characteristics, which are required for aircraft performance optimization and accurate performance prediction.

Test Results

Typical flight test results obtained from the Tornado performance test program are presented and discussed in the following sections. All flight data were generally corrected to defined standard reference conditions in order to make test data (obtained from different flights) comparable with each other or with predictions. This data reduction procedure includes correction for altitude (Reynolds number), center of gravity position and power effects. However, test flights were normally performed close to the reference conditions to keep correction terms as small as possible.

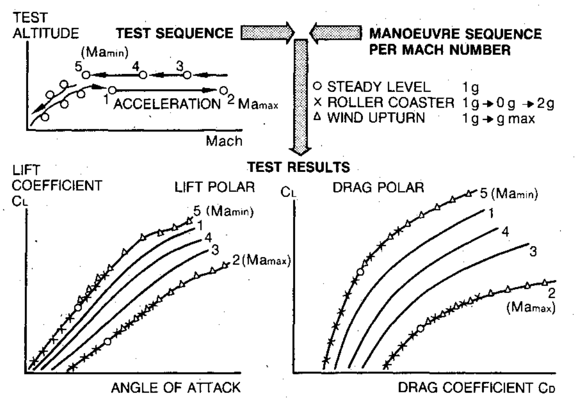

Fig. 6 Test technique.

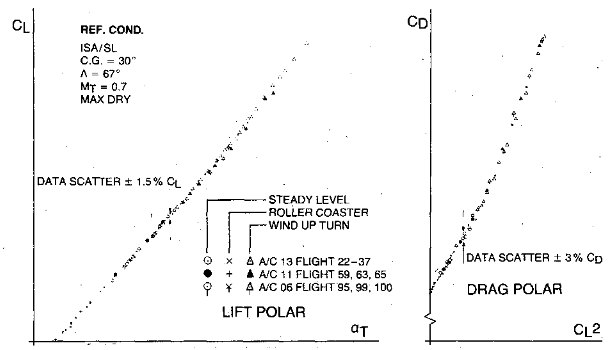

Fig. 7 Repeatability of flight test data.

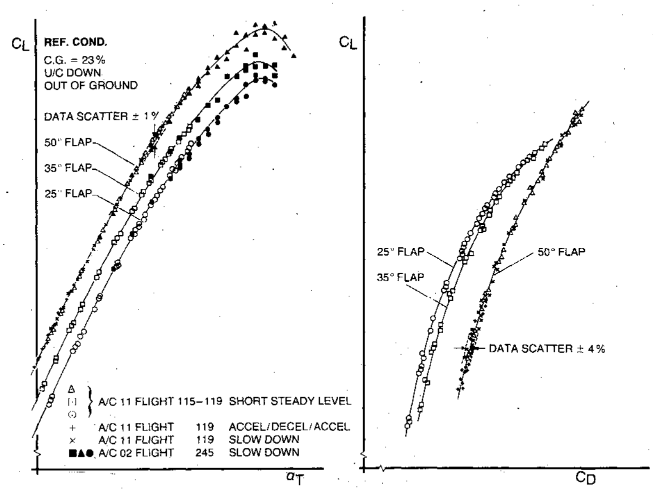

Fig. 8 Low-speed polars/high lift configuration.

Repeatability of Test Data

Figures 7 and 8 show typical lift and drag polars for the cruise and takeoff/landing configurations which were measured on three different test aircraft, however, with the same airframe standard as far as performance is concerned. For example, flight test data collected for a wing sweep of 67 deg at $Ma = 0.7$ fall within a scatterband of $\pm 1.5\%$ in the case of lift and $\pm 3\%$ in the case of drag (Fig. 8).

Furthermore, the results show excellent correlation between steady-state and dynamic test techniques. However, it must be emphasized that such an agreement can only be achieved if roller-coaster or wind-up turn maneuvers are performed

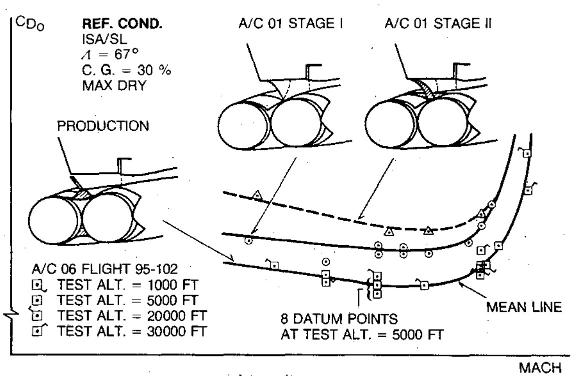

Fig. 9 Airframe optimization.

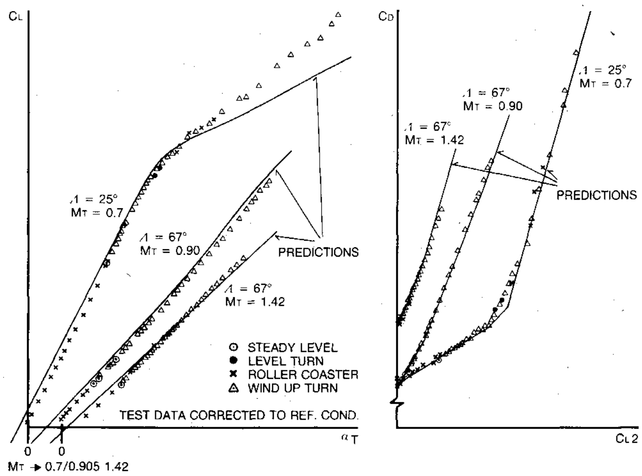

Fig. 10 Lift/drag polars, comparison flight test/prediction.

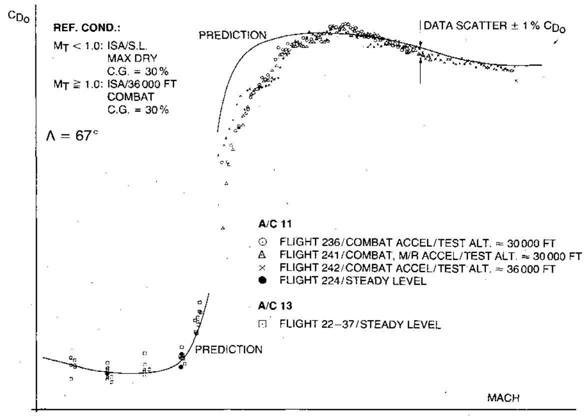

Fig. 11 Zero lift drag variation with Mach number.

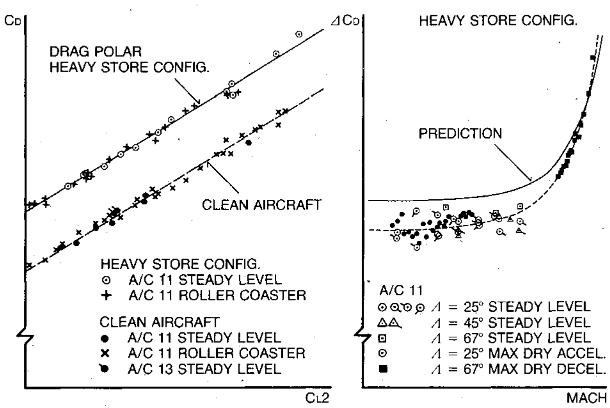

Fig. 12 External store drag.

slowly and smoothly and a certain angle-of-attack/accelerometer calibration standard, as discussed above, has been attained.

Comparable results have been achieved in the case of low-speed polars for different flap settings, as presented in Fig. 8. Again, test data obtained from steady levels, acceleration-deceleration maneuvers, and from slow-downs agree very well.

Stall test results from aircraft A/C 2 (with special test equipment, i.e., antispin chute, etc.) are also given in this figure. It is a matter of course that the data scatter will increase under stall conditions (pilot stick inputs due to wing rock, vibration, etc.). However, it was possible to define the maximum lift with a high reliability owing to the large quantity of test data derived from slow-downs.

Airframe/Optimization

As already mentioned at the beginning, the test method, as outlined in this paper, was used for a number of performance investigations in order to measure the effect of aerodynamic changes on lift and drag. An example is given in Fig. 9.

This figure shows the airplane zero lift drag variation with Mach number for aircraft A/C 1, (unfavorable rear end) and for aircraft A/C 6 (improved afterbody shape and excrescences). The zero lift drag at a given Mach number was determined from measured C_D vs C_L^2 curves, as shown in Fig. 7. In all cases the airplane induced drag characteristics were obtained from roller-coaster and wind-up turn maneuvers.

The quality and quantity of these drag measurements give evidence to the overall drag change due to airframe modifications. It was possible, as shown in Fig. 9, to reduce the drag level of A/C 6 by about 8%, which was later confirmed by drag measurements on A/C 11 as well as A/C 13.

Comparison with Predictions

Some representative comparisons between flight data and predictions follow. The predictions are based on wind-tunnel results which were adjusted from model-test to full-scale conditions.

Figure 10 shows subsonic and supersonic lift/drag polars at $Ma = 0.7$ for 25-deg wing sweep and at $Ma = 0.9$ and 1.42 for 67-deg wing sweep. Such polar measurements have been carried out for four different wing sweeps in 0.05 or 0.1 Mach increments within the entire envelope. This allows the accurate determination of drag variation with Mach number. Again the large quantity and high quality (low data scatter) of test data obtained from dynamic maneuvers permit an accurate assessment of the polar which would not be possible using steady-state maneuvers only.

In general, comparison between flight test data and predictions have shown good agreement for all wing sweeps. Minor discrepancies were found in the lift and induced drag of the 25-deg wing.

Figure 11 presents the zero lift drag variation with Mach number. The C_{D_0} figures, at a given Mach number, were determined from the basic C_D vs C_L^2 curves, as given, for example in Fig. 11. The comparison shows excellent agreement in the subsonic and higher supersonic range. Flight data show a somewhat steeper drag rise in the transonic area, but lower drag in the low supersonic Mach range.

Figure 12 shows typical results of store drag measurements for a heavy store configuration. The measured total aircraft drag as compared to the basic drag polar of the clean aircraft is given, for the most interesting angle of attack range, on the left-hand side of Fig. 12. After both polars have been corrected to the same reference conditions, the difference between the two polars represents the drag increment due to external stores. Results from measurements at different Mach numbers are plotted on the right-hand side of Fig. 12 and are compared with predictions.

Concluding Remarks

Experience gathered in the course of an extensive performance test program has shown that, using test methods currently in existence, it is possible to measure lift and drag polars accurately in-flight.

The use of dynamic maneuvers allows a drastic reduction in flying time as well as the measurement of the induced drag and zero lift drag characteristics of an aircraft. This, in turn, makes it feasible to verify in-flight, over the entire angle-of-attack range, the effects of aerodynamic modifications on lift and drag.

To achieve the indicated accuracies, high demands are placed on the flight test instrumentation, which must be specifically tailored to the task, as well as on the calibration standard of the engines involved in the thrust in-flight determination.

It is self-evident that demands of this type necessitate certain expenditures. This aspect is therefore currently the subject of an intensive effort to further improve the cost effectiveness of the flight test of the future.

Acknowledgments

The tasks of the Tornado Overall Flight Test Program are shared among Aeritalia at Caselle/Turin, British Aerospace at Warton, and Messerschmitt-Bölkow-Blohm at the Flight Test Center at Manching. The author wishes to thank his colleagues at AIT, BAe, and MBB for their close cooperation during the various segments of the Tornado performance test phases.

Reference

[1] Zeidler, V., "Performance Assessment of an Advanced Reheat Turbo Fan Engine," AIAA Paper 81-2447, Nov. 1981.